NOTES AND CORRESPONDENCE

Mesoscale Model Initialization of the Fourier Method for Mountain Waves

JOHN LINDEMAN,* DAVE BROUTMAN,+ STEPHEN D. ECKERMANN,# JUN MA,+ JAMES W. ROTTMAN,@ AND ZAFER BOYBEYI*

*College of Science, George Mason University, Fairfax, Virginia
+Computational Physics, Inc., Springfield, Virginia
#Space Science Division, Naval Research Laboratory, Washington, D.C.
@Naval Hydrodynamics Division, Science Applications International Corporation, San Diego, California

(Manuscript received 18 June 2007, in final form 26 December 2007)

ABSTRACT

A Fourier method is combined with a mesoscale model to simulate mountain waves. The mesoscale model describes the nonlinear low-level flow and predicts the emerging wave field above the mountain. This solution serves as the lower boundary condition for the Fourier method, which follows the waves upward to much higher altitudes and downward to the ground to examine parameterizations for the orography and the lower boundary condition. A high-drag case with a Froude number of ⅔ is presented.

1. Introduction

The Fourier method and the mesoscale model have long been used separately to study mountain waves (Baines 1995). The Fourier method describes only linear processes, including refraction by a vertically varying background, three-dimensional dispersion, and diffraction near caustics. Certain nonlinear processes, such as wave breaking or saturation, can be parameterized to some extent in a linear framework (e.g., Fritts et al. 2006), as they are for the linear parameterizations of subgrid-scale orographic gravity wave drag (OGWD) in climate and weather models (Kim et al. 2003). The mesoscale model, on the other hand, describes the full nonlinear response to flow over orography, including wave–wave interactions and such low-level effects as flow blocking, flow separation, and vortex shedding (e.g., Doyle et al. 2000).

An advantage of the Fourier method is that it is much faster computationally than the mesoscale model, even when run at better resolution, over broader domains, and to higher altitudes. There is also an interpretative advantage, since parts of the mountain-wave spectrum can be isolated in the Fourier method and studied independently for their contribution to the overall wave field. Waves that are vertically trapped, vertically propagating, approaching critical layers, or tunneling through wind jets can be identified and separately analyzed (e.g., Eckermann et al. 2006b).

In this paper, we examine a way to use the Fourier method in situations in which the low-level flow and orographic forcing are nonlinear. The calculation is split up so that the mesoscale model simulates only the near-surface flow and the quasi-stationary waves that emerge immediately above the mountain. Since this requires shorter time integrations over a limited height range, the resulting computational savings can be invested in high-resolution simulations that better capture the full spectrum of relevant dynamics near the mountain. The computationally faster Fourier method then propagates the mountain waves upward to higher altitudes. We are assuming that at some height just above the mountain, the mesoscale model solution is dominated by quasi-linear, quasi-stationary, upward-propagating mountain waves. This solution serves as the lower boundary condition for the Fourier method. The approach is depicted schematically in Fig. 1.

In this initial investigation, we keep things simple and consider an example with a uniform background. The

Corresponding author address: John Lindeman, College of Science, George Mason University, 4400 University Dr., Fairfax, VA 22030-4444.
E-mail: jlindema@gmu.edu

DOI: 10.1175/2008JAS2541.1

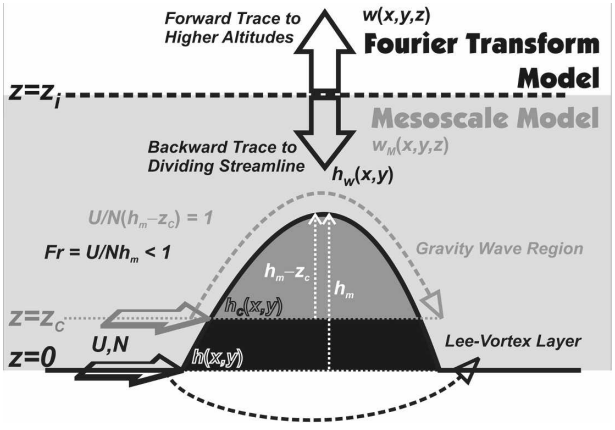

FIG. 1. A mesoscale model simulates the nonlinear near-surface flow and predicts a vertical velocity $w_M(x, y, z)$ that is used to initialize the Fourier method at height z_i. The Fourier method propagates the waves upward to higher altitudes and downward to the dividing streamline height z_c to find the wave orography h_w. See text for notation.

example has a Froude number of ⅔ and was studied numerically by Schär and Durran (1997).

At Froude numbers below unity, the linearized lower boundary condition commonly used in the Fourier method is inappropriate. This is because the streamlines near the ground tend to pass around a three-dimensional mountain or are blocked upstream by a two-dimensional mountain. Only at higher levels does the flow pass over the mountain to generate waves, and thus only some fraction of the total pressure drag across the mountain translates into a gravity wave response. The linearized lower boundary condition translates all of the pressure drag into a gravity wave response.

There are modifications of the linearized lower boundary condition that attempt to partition the total pressure drag into components due to low-level blocking/vortices and mountain waves. These are used in parameterizations of OGWD and in mountain-wave forecasting models (e.g., McFarlane 1987; Scinocca and McFarlane 2000; Webster et al. 2003; Eckermann et al. 2006a). It is unclear how (or even if) one can improve these parameterizations by further refinements to the linearized lower boundary condition. This is an important practical issue to resolve, for which the present approach might be of some use. The Fourier method can propagate the mountain waves back down to the surface from the height of initialization by the mesoscale model to infer the effective "wave orography" responsible for forcing the emergent wave fields under the assumptions of linear forcing and linear propagation. Such experiments might provide valuable objective information for improving subgrid-scale linear OGWD parameterizations and OGW forcing algorithms at moderate to low Froude number. Here we infer the wave orography for the problem of Schär and Durran (1997).

2. Model experiments

a. Problem

Following Schär and Durran (1997), we consider a uniform (unsheared) flow impinging upon a three-dimensional mountain of the form

$$h(x, y) = h_m a^3/(x^2 + y^2 + a^2)^{3/2}, \quad (1)$$

where (x, y) are the horizontal Cartesian coordinates. We set the mountain width $a = 10$ km and the maximum height $h_m = 1.5$ km. The Froude number is defined as

$$\mathrm{Fr} = U/Nh_m, \quad (2)$$

where U is the horizontal wind speed and N is the buoyancy frequency. As in Schär and Durran (1997), we choose $U = 10$ m s^{-1}, directed along the x axis, and $N = 0.01$ s^{-1}, so that Fr = ⅔.

Schär and Durran (1997) also performed two experiments with $h_m = 3$ km (Fr = ⅓). While we modeled all three experiments with similar success using our approach, we report results only for Fr = ⅔.

b. Mesoscale model

We use version 2.2 of the Weather Research and Forecasting Model (WRF) described in Skamarock et al. (2005). The model is compressible, with fifth-/third-order finite differences for the horizontal/vertical advection, and third-order Runge–Kutta for the time step.

The computational domain is 300 km × 300 km in the horizontal, with a horizontal grid spacing of 1 km and radiative lateral boundary conditions. The lower boundary is free-slip. The vertical grid spacing increases gradually from about 100 m at the ground to about 200 m at $z = 15$ km. The upper boundary is a rigid lid at $z = 30$ km, but for $z = 15$–30 km we impose vertically increasing Rayleigh damping as a sponge layer. There are 150 vertical grid points, of which 23 are in the sponge layer. Turbulent kinetic energy (TKE) is calculated prognostically, as part of a 1.5-order turbulent closure scheme. (A first-order closure scheme produced a similar wave field.) The model was run dry using the constant background wind and stratification as the initial condition.

c. Fourier method

In the Fourier method, the vertical velocity w is given by

$$w(x, y, z) = \int_{-\infty}^{\infty} \int_{-\infty}^{\infty} \tilde{w}(k, l, z) \exp[i(kx + ly)]\, dk\, dl, \tag{3}$$

where, in a uniform background,

$$\tilde{w}(k, l, z) = [\rho(z_i)/\rho(z)]^{1/2} \tilde{w}_0(k, l) \exp[im(z - z_i)]. \tag{4}$$

This includes an anelastic scaling by the inverse square root of the mean density ρ. The vertical wavenumber m satisfies the gravity wave dispersion relation

$$m^2 = (k^2 + l^2)(N^2/\hat{\omega}^2 - 1), \tag{5}$$

where k and l are the horizontal wavenumber components. The waves have upwind phase propagation ($k < 0$) and upward group propagation ($m < 0$). We omit compressibility and anelastic terms from (5), since tests with these terms retained reveal no significant difference to the results given below. We consider stationary waves only, so the intrinsic frequency $\hat{\omega} = -kU$. The effects of wave transience have been included by the method of Broutman et al. (2006).

At Froude numbers that are greater than unity, the linearized lower boundary condition is often used: $\eta(x, y, z_i) = h(x, y)$, where η is the vertical displacement of the mountain waves, and the initialization height is usually taken to be $z_i = 0$. In converting to w, this becomes $w(x, y, z_i) = Uh_x(x, y)$, or in Fourier space,

$$\tilde{w}(k, l, z_i) = -i\hat{\omega}\tilde{h}(k, l), \tag{6}$$

where $\tilde{h}(k, l)$ is the Fourier transform of $h(x, y)$.

For Froude numbers of less than unity, the linearized lower boundary condition (6) fails by incorrectly assigning all the pressure drag across the mountain to the waves. One approach to correcting (6) involves the dividing streamline, defined as the upstream height z_{ds} that separates flow around the mountain ($z < z_{ds}$) from flow over the mountain ($z > z_{ds}$). A simple calculation, shown schematically in Fig. 1, associates z_{ds} with the altitude z_c where the reduced or clipped (from below) mountain height $h_m - z_c$ yields a Froude number $N/U(h_m - z_c)$ equal to unity. For constant U and N, this gives

$$z_c = (1 - \mathrm{Fr})h_m, \tag{7}$$

an expression identical to the Sheppard criterion used as a rough guide for locating dividing streamlines in numerical model and tank experiments (e.g., Snyder et al. 1985; Baines and Smith 1993). In our problem, $z_c = 500$ m.

This in turn suggests using a linearized boundary condition at $z_i = z_c$ that retains only the clipped part of the mountain that rises above z_c. If one defines

$$h_c(x, y) = \max[h(x, y), z_c] \tag{8}$$

to be this clipped topography above z_c, the modified lower boundary condition for moderate to low Froude number flow is then

$$\tilde{w}(k, l, z_c) = -i\hat{\omega}\tilde{h}_c(k, l). \tag{9}$$

Here $\tilde{h}_c(k, l)$ is the Fourier transform of $h_c(x, y)$. The use of clipped orography to initialize a linear gravity wave model is built into a number of subgrid-scale OGWD parameterizations (e.g., McFarlane 1987; Scinocca and McFarlane 2000; Webster et al. 2003) as well as the ray-based mountain-wave forecasting model of Eckermann et al. (2006a).

A third way to initialize the Fourier method is with the mesoscale model solution. We choose an initialization height z_i just above the major nonlinearities in the low-level orographic flow. We initialize at a sufficiently long time t_i that the mesoscale model's vertical velocity, $w_M(x, y, z_i, t_i)$, is dominated by a steady-state mountain-wave response. We use vertical velocity since its variance should be dominated by gravity waves rather than by larger-scale quasi-horizontal motions (e.g., Worthington and Thomas 1998). This lower boundary condition is then

$$\tilde{w}(k, l, z_i) = \tilde{w}_M(k, l, z_i, t_i), \tag{10}$$

where $\tilde{w}_M$ is the Fourier transform of w_M.

3. Results

Figure 2 shows two Fourier solutions for w at $z = 14$ km. The solution in the left panel is initialized with the linearized lower boundary condition in (6), using $h(x, y)$ given by (1) and imposed at $z_i = 0$. The solution in the right panel is initialized with the modified lower boundary condition in (9), using the clipped orography $h_c(x, y)$ given by (8) and imposed at $z_i = z_c = 500$ m, the estimated upstream height of the dividing streamline. The solutions for w in each of these two cases have comparable peak amplitudes, presumably because w scales with the slope of the mountain, and the maximum slope is similar for the clipped and full mountains. A calculation of the vertical displacement of the mountain waves (not shown) gives peak values roughly proportional to the maximum mountain height. That is, the maximum vertical displacement for the clipped mountain is about ⅔ of the maximum value for the full mountain.

To initialize the Fourier method with the WRF model, we choose an initialization time t_i of 6 h. A time

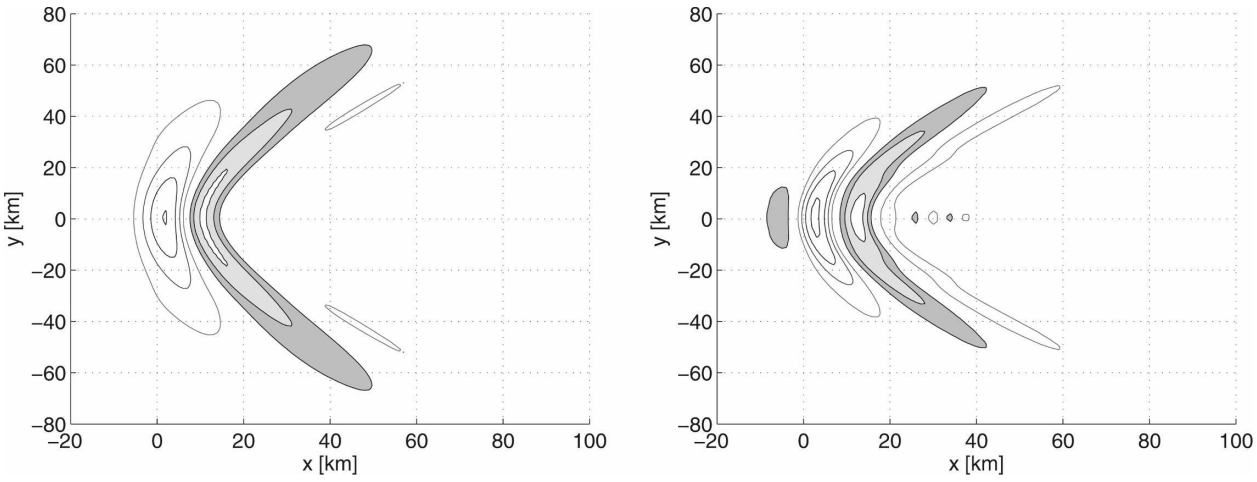

FIG. 2. (left) The Fourier solution for w at $z = 14$ km initialized with the linearized lower boundary condition in (6). Values range from -1.21 to 0.95 m s^{-1}. (right) The Fourier solution initialized by the dividing streamline method in (9). Values range from -1.28 to 1.04 m s^{-1}. The contour interval in both plots is 0.3 m s^{-1}. Here and in subsequent figures the shaded contours have positive values and the zero contour is omitted.

of 3 h would have sufficed for the initialization itself, but the longer time allowed the WRF wave fields to propagate to higher altitudes where they could be compared with the Fourier solution.

To set z_i we examine the WRF TKE fields (see section 2b). WRF generated significant TKE at heights below about 4 km (see Fig. 3), along with an associated unstable potential temperature gradient. Such TKE values are indicative of wave breaking and were noted by Schär and Durran (1997, see their Fig. 3c). We thus choose $z_i = 5$ km. The WRF solution $w_M(x, y, z_i, t_i)$ at $z_i = 5$ km and $t_i = 6$ h is plotted in Fig. 4. This is the lower boundary condition for the Fourier method.

The WRF solution $w_M(x, y, z, t_i)$ at $z = 14$ km is shown in the left panel of Fig. 5. The right panel shows the corresponding Fourier solution initialized by the WRF solution in Fig. 4. Corresponding vertical cross sections at $y = 0$ are plotted in Fig. 6 for the WRF solution (left panel) and for the WRF-initialized Fourier solution (right panel). These results reveal good overall agreement, indicating that the WRF initialization provides a much better reproduction of the wave field, in amplitude and spatial extent, than the linear solutions of Fig. 2. Despite the low-level turbulent dissipation in the WRF simulation (see Fig. 3), the waves emerge with larger amplitude than in the linear cases of Fig. 2.

The WRF initialization at $z_i = 5$ km can also be used to calculate the Fourier solution at heights below z_i. The right panel of Fig. 6 shows the result of extending the Fourier solution to both higher and lower altitudes. The point of the calculation at lower altitudes is to infer the wave orography h_w consistent with linear boundary forcing of the waves observed in the WRF simulation. If the dividing streamline idea were accurate, the Fourier solution initialized by WRF at height z_i and then propagated downward to height z_c should yield an estimate of h_w that resembles the clipped orography h_c used in (8). Since at $z = 14$ km, the Fourier solution initialized using h_c differs from the WRF solutions (c.f. Figs. 2 and 5), this suggests that h_w should differ from h_c.

To test this, we estimate

$$h_w(x, y) = \eta(x, y, z_c) + z_c, \tag{11}$$

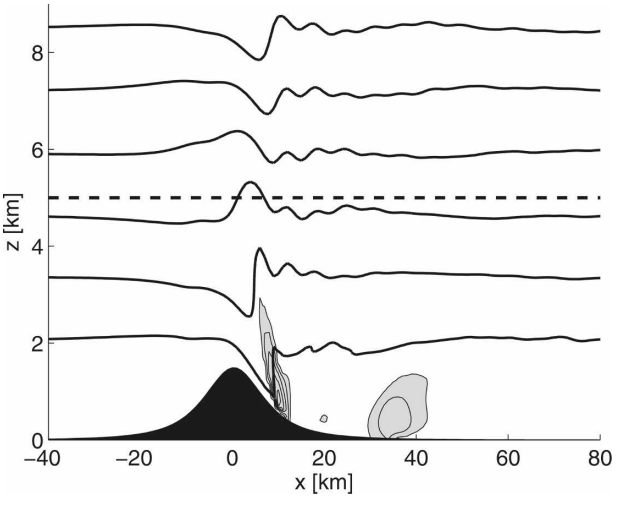

FIG. 3. The WRF solution for TKE (shaded contours) at $y = 0$. Values range from 0 to 5.8 m^2 s^{-2}, with a contour interval of 1 m^2 s^{-2}. Thick solid lines show the isentropes from the WRF solution, starting at 294 K and increasing in intervals of 4 K with height. The dashed line at $z = 5$ km indicates the initialization height z_i for the Fourier method.

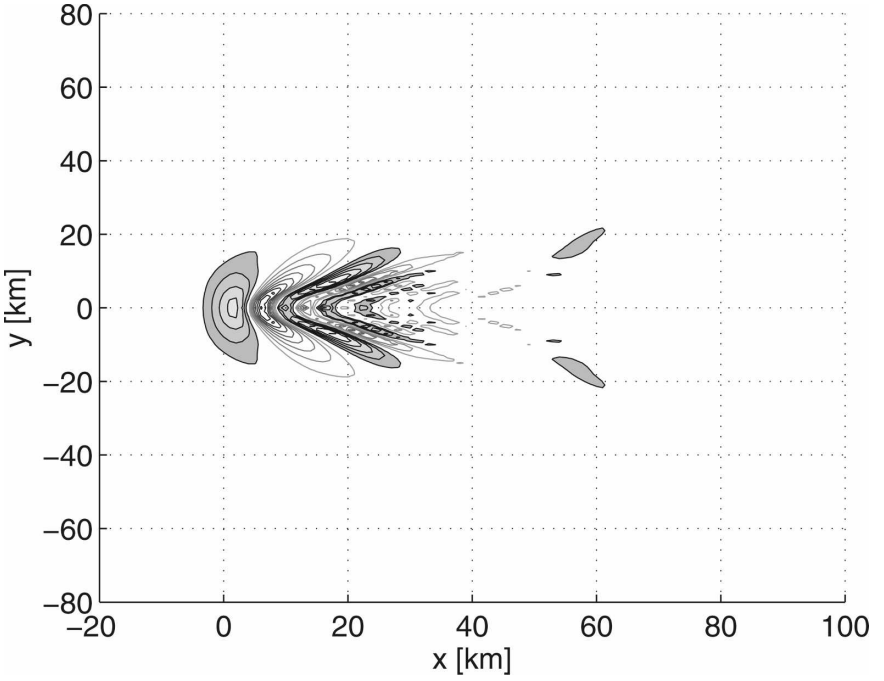

FIG. 4. The WRF solution for w at $z = 5$ km, used as the lower boundary condition for the Fourier method. Values range from -2.65 to 1.82 m s^{-1}, with contour interval 0.3 m s^{-1}.

where η is the WRF-initialized Fourier solution for vertical displacement evaluated at the estimated height $z_c = 500$ m of the upstream dividing streamline.

Contour plots of $h_w(x, y)$ and $h_c(x, y)$ are shown in the left and right panels of Fig. 7, respectively. A one-dimensional slice through these topographies at the centerline $y = 0$ is shown in the left panel of Fig. 8. We see particularly from Fig. 8 that, on the upstream side of the topography, h_w and h_c have similar shape and height, although h_w is slightly taller and somewhat wider at its base.

On the downstream side, h_w differs noticeably from both h_c and h, dropping rapidly from its peak value and then oscillating a couple of times about a height of ~500 m. The nonlinearity of the low-level flow downstream of the obstacle is the likely origin of this shape.

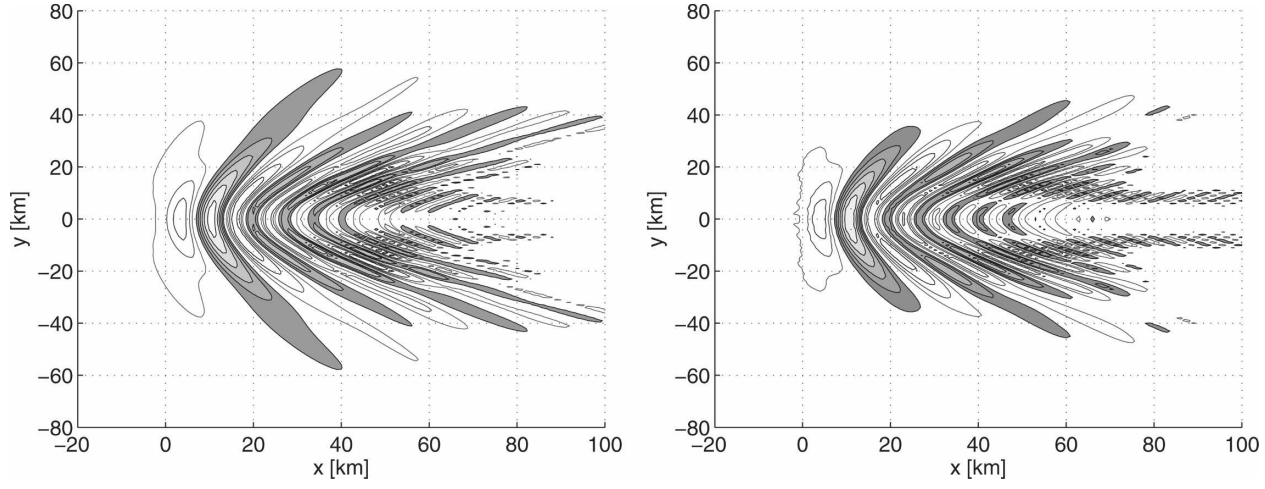

FIG. 5. The solution for w at $z = 14$ km computed by the (left) WRF model and (right) Fourier method. The Fourier solution is initialized at $z_i = 5$ km with the WRF solution of Fig. 4. Values range from -1.50 to 1.87 m s^{-1} for the WRF model and from -1.41 to 1.95 m s^{-1} for the Fourier solution. The contour interval is 0.3 m s^{-1}.

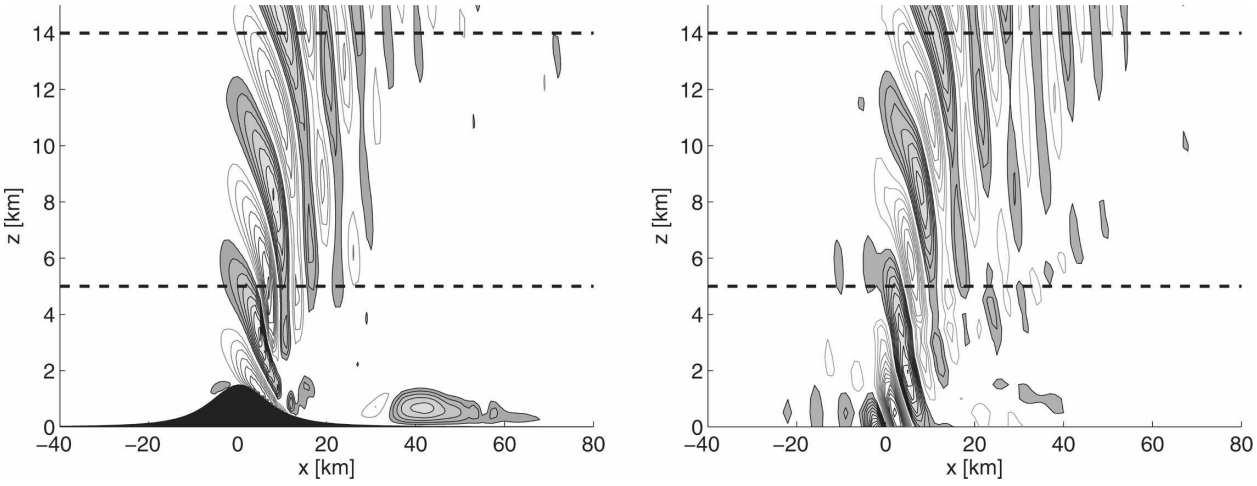

FIG. 6. (left) The WRF solution for w at $y = 0$, the centerline of the mountain. Dashed lines indicate the initialization height for the Fourier method ($z_i = 5$ km) and the height at which the WRF and Fourier solutions are compared in Fig. 5 ($z = 14$ km). The contour interval is 0.3 m s^{-1}. The sponge layer begins at 15 km. (right) The corresponding Fourier solution.

For example, in the WRF simulations the streamlines passing over the mountain are not symmetric about $x = 0$, but exhibit a steep drop in the lee that triggers a leeside surface wind maximum and the TKE shown in Fig. 3 here and in Fig. 3c of Schär and Durran (1997). To the Fourier model, such distortions act as a modification to the effective obstacle shape, which is reflected in the h_w fields recovered from the backtraced Fourier solutions in Figs. 7 and 8.

To study this further, the corresponding amplitude spectra of h, h_c, and h_w are shown in the right panel of Fig. 8. These are obtained by discrete Fourier transform of the orographic cross sections shown in the left panel. Since the functional form of $h(x, y)$ in (1) is smooth, its spectrum decreases exponentially at the large mode numbers shown in the plot. Since h_c is clipped, its spectrum has high-mode-number Gibbs oscillations whose amplitude decreases as the mode number to the -2 power.

The spectrum of the h_w cross section vanishes abruptly after mode number 47. These higher mode numbers force vertically evanescent gravity waves, whose energy is not recovered by the free downward propagation of the Fourier solution using the $z_i = 5$ km WRF solution. Mode 47 corresponds to a cutoff wavelength of about 6.4 km, and this corresponds to the scale of the short oscillations in h_w seen in the left panel of Fig. 8. At mode numbers ~20–47 (wavelengths ~6–15 km), the spectrum for h_w is enhanced relative to the spectra for h and h_c. The enhanced variance at these

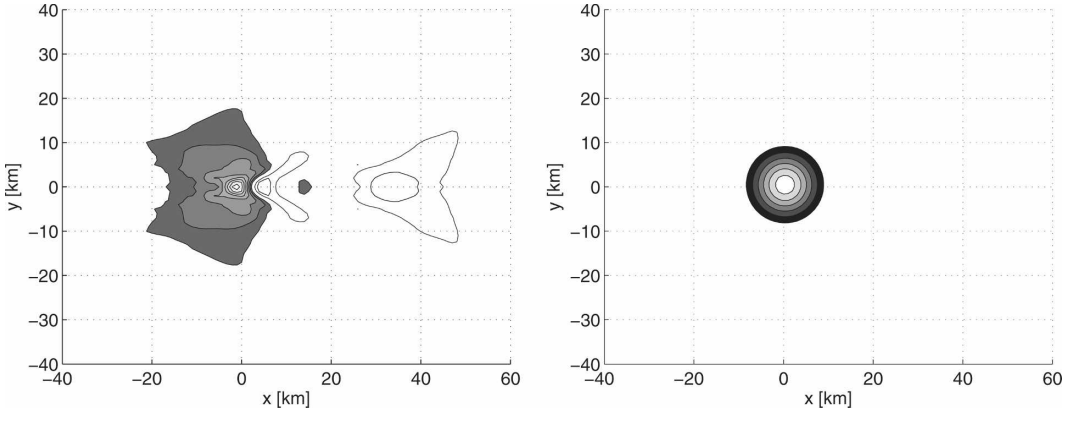

FIG. 7. (left) The Fourier solution in (11) for the wave orography h_w at the height of the dividing streamline, 500 m. Values range from 44 to 1799 m, and shaded contours represent heights above 500 m. (right) The clipped topography h_c. Values range from 500 to 1500 m. The contour interval in both plots is 150 m.

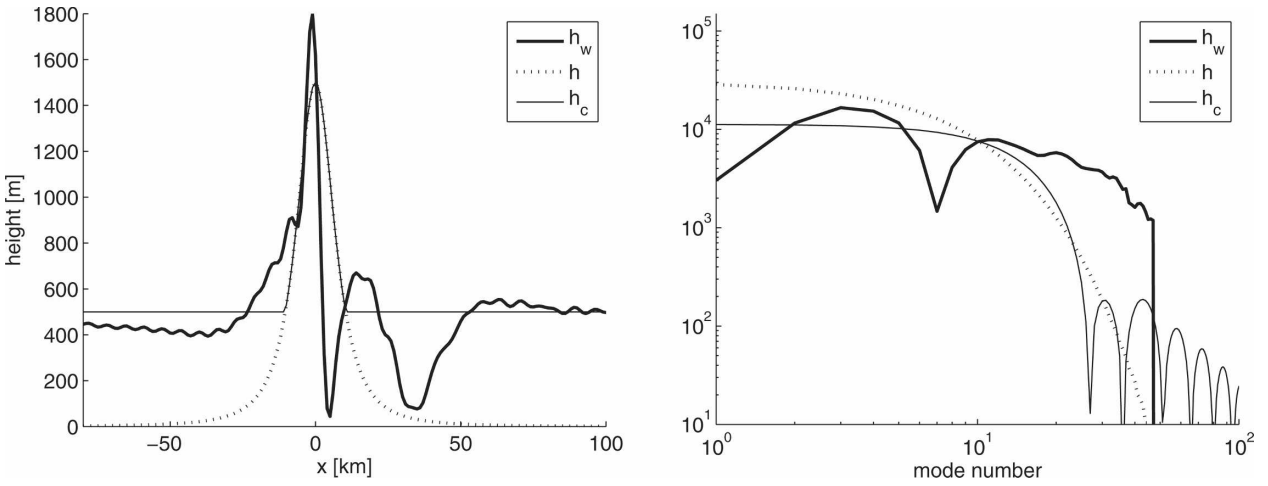

FIG. 8. (left) The wave orography h_w of Fig. 7 along the centerline $y = 0$, indicated by the thick line. Also plotted are h of (1) and h_c of (8). (right) The amplitude spectrum for each curve in the left panel. Mode number 1 refers to a wavelength of 300 km.

scales in the h_w spectrum is apparent in wave structure of similar horizontal scales in the wave field solutions in Figs. 5 and 6. We also calculated the wave orography h_w at $z = 0$ and $z = 1000$ m and found similar features.

4. Summary

We considered mountain waves generated by a three-dimensional mountain for a Froude number of ⅔. The Fourier solution with the linearized lower boundary condition for orographic forcing did not accurately describe the wave field predicted by a nonlinear mesoscale model. When initialized instead with the mesoscale model solution at a single height above the major nonlinearity in the low-level flow, the Fourier method reproduced the mountain waves much more accurately. The Fourier method initialized in this way can also propagate the wave field from the initialization height back down toward the ground, as we have done to produce Figs. 6–8. The purpose of this is to help to determine a parameterized orography and lower boundary condition consistent with the wave field at higher altitudes and the linearized equations for wave propagation. Subgrid-scale OGWD parameterizations in global weather and climate models use this kind of approach (e.g., Scinocca and McFarlane 2000; Webster et al. 2003), as does the ray-based mountain-wave forecast model of Eckermann et al. (2006a).

We calculated the mesoscale model solution up to a height of 15 km, with a 15-km sponge layer above that. This height range was chosen to demonstrate good agreement with the Fourier solution. If we had needed the mesoscale model only to initialize the Fourier solution, we could have used a somewhat shallower domain. Note that Schär and Durran (1997), whose low-level results we have reproduced, simulated this case with a model height of only 12 km (and a radiation condition at 12 km). In another example that might be suitable for our approach, Lane et al. (2006) simulated winds over the island of Kauai with a model that extended only 10 km high (with an 8-km sponge layer above that).

The results here suggest that our method has potential for efficiently propagating high-resolution tropospheric mountain-wave fields to much higher altitudes (e.g., into the stratosphere and mesosphere) and into much broader horizontal domains. Realistic winds and stratification can be handled as in Eckermann et al. (2006b). However, the wave field can become nonlinear as it propagates upward, and a parameterization for wave breaking will be need to be implemented.

While we have focused on mountain-wave problems, the method can potentially be extended to other sources of gravity waves. The complexity of wave generation by convection and jet stream imbalance, for instance, often requires mesoscale model simulations. Several studies have spectrally analyzed the output of such simulations to characterize the amplitudes, wavelengths, and phase speeds of the gravity waves radiating away from these sources, and then have propagated these wave groups to higher altitudes using spatial ray methods (e.g., Alexander 1996; Vadas and Fritts 2004; Plougonven and Snyder 2005). Other studies have backtraced model-generated wave groups at higher altitudes to infer the altitude, location, and overall nature of the source (e.g., Reeder and Griffiths 1996; Lin and Zhang 2008). Since the ray method can be formulated in Fourier space (Broutman et al. 2003, 2006), our work

may provide the basis for a systematic approach to these kinds of studies.

Acknowledgments. This work is part of the Ph.D. thesis of JL. Funding was provided for JL and DB by the National Science Foundation under Grants ATM-0448888 and ATM-0435789; for SDE by the Office of Naval Research 6.1 program and by NASA's Modeling, Analysis and Prediction program, Grant NNG06HM19i; and for JM by MDA Contract B044-159-0300.

REFERENCES

Alexander, M. J., 1996: A simulated spectrum of convectively generated gravity waves: Propagation from the tropopause to the mesopause and effects on the middle atmosphere. *J. Geophys. Res.,* **101,** 1571–1588.

Baines, P. G., 1995: *Topographic Effects in Stratified Flows*. Cambridge University Press, 482 pp.

——, and R. B. Smith, 1993: Upstream stagnation points in stratified flow past obstacles. *Dyn. Atmos Oceans.,* **18,** 105–113.

Broutman, D., J. W. Rottman, and S. D. Eckermann, 2003: A simplified Fourier method for nonhydrostatic mountain waves. *J. Atmos. Sci.,* **60,** 2686–2696.

——, J. Ma, S. D. Eckermann, and J. Lindeman, 2006: Fourier-ray modeling of transient trapped lee waves. *Mon. Wea. Rev.,* **134,** 2849–2856.

Doyle, J. D., and Coauthors, 2000: An intercomparison of model-predicted wave breaking for the 11 January 1972 Boulder windstorm. *Mon. Wea. Rev.,* **128,** 901–914.

Eckermann, S. D., A. Dörnbrack, S. B. Vosper, H. Flentje, M. J. Mahoney, T. P. Bui, and K. S. Carslaw, 2006a: Mountain wave–induced polar stratospheric cloud forecasts for aircraft science flights during SOLVE/THESEO 2000. *Wea. Forecasting,* **21,** 42–68.

——, D. Broutman, J. Ma, and J. Lindeman, 2006b: Fourier-ray modeling of short wavelength trapped lee waves observed in infrared satellite imagery near Jan Mayen. *Mon. Wea. Rev.,* **134,** 2830–2848.

Fritts, D. C., S. L. Vadas, K. Wan, and J. A. Werne, 2006: Mean and variable forcing of the middle atmosphere by gravity waves. *J. Atmos. Sol.-Terr. Phys.,* **68,** 247–265.

Kim, Y.-J., S. D. Eckermann, and H.-Y. Chun, 2003: An overview of the past, present and future of gravity-wave drag parametrization for numerical climate and weather prediction models. *Atmos.–Ocean,* **41,** 65–98.

Lane, T., R. D. Sharman, R. G. Frehlich, and J. M. Brown, 2006: Numerical simulations of the wake of Kauai. *J. Appl. Meteor. Climatol.,* **45,** 1313–1331.

Lin, Y., and F. Zhang, 2008: Tracking gravity waves in baroclinic jet-front systems. *J. Atmos. Sci.,* **65,** 2402–2415.

McFarlane, N. A., 1987: The effect of orographically excited gravity wave drag on the general circulation of the lower stratosphere and troposphere. *J. Atmos. Sci.,* **44,** 1775–1800.

Plougonven, R., and C. Snyder, 2005: Gravity waves excited by jets: Propagation versus generation. *Geophys. Res. Lett.,* **32,** L18802, doi:10.1029/2005GL023730.

Reeder, M. J., and M. Griffiths, 1996: Stratospheric–inertia gravity waves generated in a numerical model of frontogenesis. II: Wave sources, generation mechanisms, and momentum fluxes. *Quart. J. Roy. Meteor. Soc.,* **122,** 1175–1195.

Schär, C., and D. R. Durran, 1997: Vortex formation and vortex shedding in continuously stratified flows past isolated topography. *J. Atmos. Sci.,* **54,** 534–554.

Scinocca, J. F., and N. A. McFarlane, 2000: The parametrization of drag induced by stratified flow over anisotropic orography. *Quart. J. Roy. Meteor. Soc.,* **126,** 2353–2393.

Skamarock, W. C., J. C. Klemp, J. Dudhia, D. O. Gill, D. M. Barker, W. Wang, and J. G. Powers, 2005: A description of the advanced research WRF version 2. NCAR Tech. Note NCAR/TN-468+STR, 88 pp.

Snyder, W. H., R. S. Thompson, R. E. Eskridge, R. E. Lawson, I. P. Castro, J. T. Lee, J. C. R. Hunt, and Y. Ogawa, 1985: The structure of strongly stratified flow over hills: Dividing streamline concept. *J. Fluid Mech.,* **152,** 249–288.

Vadas, S. L., and D. C. Fritts, 2004: Thermospheric responses to gravity waves arising from mesoscale convective complexes. *J. Atmos. Sol.-Terr. Phys.,* **66,** 781–804.

Webster, S., A. R. Brown, D. R. Cameron, and C. P. Jones, 2003: Improvements to the representation of orography in the Met Office Unified Model. *Quart. J. Roy. Meteor. Soc.,* **129,** 1989–2010.

Worthington, R. M., and L. Thomas, 1998: The frequency spectrum of mountain waves. *Quart. J. Roy. Meteor. Soc.,* **124,** 687–703.